AEROSPACE

INTER IIT TECH MEET 14.0

Mid-Term Report

TEAM 58
Powered Lift Wing Design Using Externally Blown Flaps with Distributed Electric Propulsion

---

Authors

Abhijit Venkat	Mechanical Engineering
Aditya Prasad	Mechanical Engineering
Diya Mehta	Mechanical Engineering
Hari Balaji	Mechanical Engineering
Kushagra Shahi	Mechanical Engineering
Kushagreek Basu	Mechanical Engineering
Mohan Ulasa	Mechanical Engineering
Sai Gawali	Mechanical Engineering

November 12, 2025

Contents

Executive Summary

Objective. Design a fixed-wing electric STOL aircraft that attains short take-off and landing performance through powered-lift (blown-wing) without VTOL or mechanical thrust-vectoring. The propulsion system is treated as an integral aerodynamic component (Distributed Electric Propulsion, DEP) to achieve high lift during take-off and landing while preserving efficient cruise.

Concept and Rationale. The selected concept is an *Externally Blown Flap (EBF)* integrated with Distributed Electric Propulsion (DEP). This choice is driven by: (i) the ability of propeller slipstreams to energize the wing/flap upper surface and delay flow separation and thus stall, (ii) higher propulsive efficiency and greater mass-flow of propellers at low flight speeds compared with EDFs, and (iii) the natural compatibility of small, spanwise-distributed propellers with uniform slipstream coverage, redundancy, and differential thrust control.

Modeling approach.

- **Analytical (primary):** Kuhn's semi-empirical method is used to predict lift augmentation for the propeller–wing–flap system. Kuhn's method combines momentum balance with empirical correction factors to represent thrust deflection, slipstream mass-flow increase and thrust recovery in the attached-flow regime -making it well suited for propeller-driven EBF–DEP conceptual design.
- **CFD (validation plan):** A two-stage CFD strategy is adopted, following validated literature practice:
    1. Rapid parametric exploration using a 2D actuator-disk model (uniform pressure rise) to map configuration space (propeller diameter, vertical/axial placement).
    2. High-fidelity 3D validation using a uniform-pressure 3D actuator-disk model (assuming no swirl) to capture spanwise effects; swirl due to the propellers will be neglected because prior studies show it has only a second-order effect on maximum lift and stall angle.
- **Actuator-disk simplification:** Propellers are modelled as circular actuator disks (diameter chosen from propeller database) and implemented as a momentum source (fan model) in CFD -consistent with momentum-based assumptions in Kuhn's approach and dramatically reducing runtime.

Key Preliminary Calculations and Design Point.

- The selected airfoil for the powered-lift configuration is the **Eppler E423**, chosen for its high camber and favorable low-speed characteristics that yield high lift coefficients at moderate angles of attack.
- The example design case considers the following fixed parameters: number of propellers $N = 6$, aspect ratio $AR = 10$, flap-to-chord ratio $B = 0.12$, geometric angle of attack $\alpha = 12°$,

slipstream turning angle $\theta = 60°$, total available thrust $T_{tot} \approx 96$ N, free-stream velocity $V_\infty = 20$ m/s, and air density $\rho = 1.225$ kg/m^3.

- Solving the modified Kuhn lift relation (Eq. 15) for the design target $C_L = 8$ yields a **wing chord length** of $c_w \approx 0.11$ m. For the chosen aspect ratio and span $b = 1.1$ m, the corresponding **wing planform area** is $S = b\, c_w \approx 0.121$ m^2.
- From the geometric relation $ND = b$, the equivalent propeller diameter is determined as $D = 0.1778$ m. A matching commercially available propeller was identified from the **APC (Advanced Precision Composites)** database, producing an approximate **static thrust** of 13.34 N per unit. The total thrust from six propellers is thus $T_{tot} \approx 80.05$ N, which lies within the design thrust envelope.
- Substituting this measured thrust value into Kuhn's semi-empirical formulation gives an **effective lift coefficient** of $C_L \approx 7.76$, which is within 3% of the target $C_L = 8$. This close agreement between analytical prediction and thrust-based estimation validates the consistency of the modeling approach and the chosen design point.

CFD Status and Limitations.

- The complete 3D geometry of the wing–actuator disk assembly was generated in **Autodesk Fusion** and refined in **ANSYS Discovery** to eliminate surface discontinuities. The geometry was subsequently imported into **SimScale** for meshing and solver setup.
- The intended numerical setup employs a **steady-state, incompressible RANS solver** with the k–ω **SST turbulence model** and an **actuator-disk momentum source** to represent the propeller slipstream. The prescribed mean induced velocity through the disk is computed from the measured thrust using the actuator-disk momentum relation, ensuring physical consistency with Kuhn's semi-empirical assumptions.
- During pre-processing, the automatic **hex-dominant meshing algorithm** in SimScale encountered persistent topological inconsistencies at the disk–wing intersection. These manifested as non-manifold edges and highly skewed cells in the local volume mesh, leading to failure of surface refinement and inflation-layer generation in subsequent iterations.
- Consequently, the final mesh could not be generated within the current iteration cycle, and the numerical simulations were not executed. The issue is attributed to geometric intersection complexity and insufficient local element quality near the actuator-disk boundary.
- As a result, the **analytical predictions based on Kuhn's method** currently serve as the baseline reference for aerodynamic performance. CFD validation will be conducted once the geometry is locally simplified and an alternative meshing strategy—such as a hybrid tetrahedral–prismatic mesh or manual block-structured grid—is implemented to ensure convergence and near-wall accuracy.

Conclusions from preliminary work. The combined analytic–data workflow demonstrates internal consistency: a plausible wing chord and propeller selection satisfy the target lift coefficient using Kuhn's semi-empirical model, and available propellers produce thrust near the design envelope. Kuhn's model is appropriate for the EBF–DEP configuration and provides a fast, validated tool for concept-level sizing and parametric exploration.

Planned Next Steps (End-Term Targets).

1. **Geometry and Meshing Refinement:** Resolve existing meshing issues by (i) removing non-manifold surface intersections, (ii) simplifying the disk–wing interface geometry, and (iii) implementing alternative meshing approaches such as hybrid tetrahedral–prismatic inflation layers or manual block-structured grids to ensure near-wall mesh quality and solver convergence.

2. **Completion of CFD Campaign:** Execute the two-stage CFD analysis framework—initial 2D actuator-disk parametric sweep followed by 3D uniform-pressure simulations for selected configurations. Incorporate swirl effects only if observed discrepancies in lift or stall characteristics exceed acceptable bounds.

3. **Parametric Sensitivity Study:** Conduct systematic variation of key design parameters, including propeller count (N), propeller diameter (D), vertical offset (y_p), slipstream turning angle (θ), and flap geometry, to identify trends and define a robust operational envelope that mitigates jet detachment and stall onset.

4. **Integrated Performance Analysis:** Extend the aerodynamic model to include propulsion, mass and power coupling, preliminary weight estimation, and control-allocation logic using differential thrust. Quantify the resulting performance metrics such as take-off distance, climb rate, and cruise efficiency penalties under STOL mission constraints.

5. **Experimental Validation Planning:** Develop a preliminary wind-tunnel test plan using a reduced-scale model to validate key aerodynamic assumptions and lift-augmentation behavior once CFD results are available. Outline instrumentation, scaling laws, and target measurement parameters.

Deliverables for the next submission. (i) Fully meshed SimScale models and completed 3D uniform-pressure CFD for 2–3 optimized configurations, (ii) updated Kuhn-based sizing tables and sensitivity maps, (iii) preliminary propulsion/power budget, and (iv) a short wind-tunnel validation plan.

List of Symbols

Symbol	Description
C_L	Coefficient of lift (dimensionless)
C_D	Coefficient of drag (dimensionless)
ρ	Air density
V	Free stream velocity
α	Angle of attack
T	Thrust
W	Weight
η_p	Propeller Efficiency
θ	Angle of Deflection of Slipstream
δ_f	Flap Deflection Angle
θ_w	Slipstream Deflection by Wing
θ_f	Slipstream Deflection by Flap
N	Number of Propellers
S_p	Propeller Disc Area
AR	Aspect Ratio
q	Freestream Dynamic Pressure
c_w	Length of wing chord
c_f	Length of flap chord
δ_e	Angle between the trailing edge and the thrust direction
D	Diameter of the propeller

1 Introduction

With rapid advances in air mobility and a steady increase in urban population density, the demand for short-range, distributed, and sustainable air transport solutions has grown significantly. The vision of **Urban Air Mobility (UAM)** and **Regional Air Mobility (RAM)** requires aircraft that can operate efficiently from limited take-off and landing areas, such as short runways or even rooftop pads. Conventional fixed-wing aircraft, which depend on long runways to build up the necessary take-off speed, are not well-suited for such operations.

To address this limitation, next-generation aircraft must achieve high lift at low airspeeds while maintaining safety, efficiency, and compactness. This requirement naturally leads to the exploration of **powered-lift configurations**, where the propulsion system is actively used to enhance aerodynamic performance. The fundamental challenge is to generate sufficient lift within a constrained take-off distance, without excessively increasing power consumption or system complexity.

In conventional aircraft, lift generation relies mainly on airspeed, wing area, and airfoil geometry. However, during short take-off, the available dynamic pressure is very low, making it difficult to achieve the required lift through aerodynamic design alone. This limitation motivates the use of **lift augmentation techniques** - broadly categorized into **passive** and **active** methods.

Passive lift augmentation includes techniques such as high-lift airfoils, leading-edge slats, and trailing-edge flaps, which improve the effective camber of the wing and delay flow separation. These methods are simple and efficient but limited by the available flow energy.

Active lift augmentation, on the other hand, involves the injection or redirection of high-energy flow to modify the surrounding aerodynamics. Examples include internally blown flaps, externally blown flaps, circulation control wings (CCW), and Upper Surface Blowing (USB).

Among these, the **Upper Surface Blowing (USB)** concept is particularly attractive for electric or hybrid-electric distributed propulsion systems. In this configuration, propellers or ducted fans are placed ahead of the wing such that their slipstream flows directly over the upper surface and trailing edge. The high-momentum jet remains attached to the surface due to the **Coandă effect**, resulting in a significant increase in circulation and lift. This mechanism enables higher lift coefficients (C_L) and lower stall speeds, allowing take-off and landing from short runways.

In the present study, our focus lies on designing and analyzing a small-range aircraft with a USB configuration powered by distributed electric propellers. The objective is to determine how propeller-induced blowing can be optimized to achieve the required lift.

2 Concept Overview

The core objective of this problem statement is to design a wing for a **fixed-wing aircraft** capable of achieving **Short Take-Off and Landing (STOL)** performance through **powered lift**, without relying on **Vertical Take-Off and Landing (VTOL)** systems or complex tilting mechanisms. In this design, the **propulsion system** is not limited to providing thrust alone but also contributes directly to the generation of **aerodynamic lift**. This integration fundamentally changes the conventional ap-

proach to aircraft design, requiring the propulsion and aerodynamic systems to be treated as a **coupled unit** rather than independent components. The design therefore aims to achieve **high lift performance** during take-off and landing while maintaining **efficient cruise characteristics**, ensuring that the aircraft performs effectively across distinct flight regimes.

At low flight speeds, the available airflow energy is limited, and the boundary layer tends to separate easily, resulting in stall and a rapid loss of lift. Conventional aerodynamic techniques such as larger wings, high-lift flaps, or slats can only achieve maximum lift coefficients in the range of about **2 to 3**, which is insufficient for the lift demands of STOL operations. Increasing the wing area to overcome this limitation leads to higher drag and reduced cruise efficiency. Hence, a **powered-lift approach** that enhances lift aerodynamically without structural or mechanical complications offers a more effective and efficient solution.

The **blown-wing concept** satisfies this requirement by using **propeller or EDF slipstreams** to energize the airflow over the wing and flaps, delaying flow separation and significantly increasing lift. In this configuration, multiple small propellers are distributed along the wing's leading edge, producing a uniform, accelerated airflow across the lifting surface. This interaction enables high lift during take-off and landing while maintaining efficient cruise characteristics. The **distributed propellers** also provide improved control through **differential thrust**, enhancing handling qualities during low-speed operations. Overall, the blown-wing configuration provides the most practical and aerodynamically efficient solution to meet the problem statement's objectives, merging the advantages of **distributed electric propulsion** and **powered lift** without the structural complexity of VTOL systems.

2.1 Design Targets and Performance Requirements

- **Lift Coefficient Target (C_L): 6.5**, with an operational **envelope of 6–8**.
- **Lift-to-Drag Ratio (L/D):**
  - **> 5** with flaps deployed (take-off and landing modes)
  - **> 20** without flaps (cruise mode)
- **Minimum Lift: 15 kg at 20 m/s** freestream velocity.
- **Freestream Velocity Requirements:**
  - With flaps deployed (**take-off mode**): **20 m/s**
  - With flaps retracted (**cruise mode**): **80 m/s**
- **Thrust-to-Weight Ratio Envelope: 0.5 < T/W < 0.65**
- **Maximum Take-Off Weight (MTOW): 15 kg**

3 Rationale for Using Propellers Instead of Electric Ducted Fans

The choice of propulsive device is a critical aspect of any powered-lift or distributed electric propulsion (DEP) aircraft concept. For the present STOL configuration, **propeller-based propulsion** has been selected over electric ducted fans (EDFs) due to superior aerodynamic efficiency, lift augmentation potential, and integration feasibility in low-speed flight regimes. The following subsections outline the rationale behind this selection.

3.1 Aerodynamic Rationale

Propeller-driven systems are inherently more effective in low-speed, high-lift flight regimes. A propeller accelerates a relatively large mass of air at a moderate velocity, producing a broad, low-speed slipstream that interacts favorably with the wing and flap surfaces. This distributed slipstream energizes the boundary layer, delays flow separation, and significantly increases the effective lift coefficient ($C_{L,\max}$)-a primary requirement for powered-lift and STOL performance.

In contrast, EDFs accelerate a smaller mass of air to high velocity, resulting in a narrow jet with limited lateral spread. Such a jet contributes primarily to thrust rather than lift, as the localized high-velocity core does not provide uniform blowing across the wing span. Consequently, EDFs are aerodynamically better suited to compact, high-speed applications where lift augmentation is secondary to thrust generation, whereas propellers are optimal for distributed, low-speed, lift-enhancing configurations.

3.2 Power and Efficiency Considerations

Propeller systems exhibit higher propulsive efficiency in low- to moderate-speed flight due to their lower disk loading and higher mass flow per unit thrust. Propellers satisfy this condition by imparting small velocity increments over large disk areas, minimizing kinetic energy losses in the slipstream. This makes them ideal for electrically powered aircraft, where available energy and power density are constrained.

EDFs, by comparison, operate with very high disk loading and require substantially greater shaft power to produce equivalent thrust. Their smaller fan diameters and higher rotational speeds increase mechanical losses and motor heating, leading to reduced overall system efficiency and more complex thermal management. These factors make EDFs less favorable for DEP systems designed for low-speed, high-lift operations.

3.3 Integration with the Wing and DEP System

In distributed propulsion architectures, propellers integrate naturally with the wing structure. Multiple small-diameter propellers distributed along the wing span generate overlapping slipstreams, producing nearly continuous blowing across the wing and flap surfaces. This configuration enhances both lift and control authority while ensuring consistent boundary-layer re-energization during takeoff and landing.

Conversely, EDFs produce highly concentrated, high-speed jets with limited spatial coverage, yielding negligible aerodynamic interaction with the wing surface. As a result, EDF-based configurations would fail to provide effective lift augmentation or flow control, defeating the purpose of a blown-wing powered-lift concept.

3.4 Structural and Operational Advantages

Propeller systems offer several mechanical and operational advantages. They are structurally simpler, lighter, and more adaptable to modular DEP configurations, where each unit can be driven by an independent electric motor and controller. This distributed architecture inherently provides redundancy and fault tolerance, enhancing flight safety.

EDFs, on the other hand, operate at very high rotational speeds, imposing greater centrifugal and vibrational loads on nacelles and mounts. They require tighter manufacturing tolerances, precise balancing, and often active cooling systems, increasing both mechanical complexity and system mass. Additionally, EDFs generate higher noise levels compared to propellers, which may pose challenges for urban or small-airfield operations.

3.5 Design Suitability and Mission Alignment

The mission objectives of the present design emphasize low-speed, high-lift performance, efficient power utilization, and smooth aerodynamic integration with the wing. Propellers directly support these goals by producing large, slow-moving slipstreams that effectively energize the airflow over the wing and flap systems, thereby achieving substantial lift augmentation with limited power expenditure.

In contrast, EDFs, though compact and capable of generating high static thrust, are optimized for higher-speed aerodynamic conditions. Their high exit velocities and limited mass flow yield poor lift augmentation and low propulsive efficiency at low speeds. Therefore, propeller-driven distributed electric propulsion provides a more effective and energy-efficient solution aligned with the performance and mission requirements of the current STOL design.

4 Overview of Passive Lift-Augmentation Methods

Passive lift-augmentation techniques rely on geometric modification and aerodynamic shaping of the lifting surfaces to enhance lift without the addition of external energy to the flow. These methods improve aerodynamic performance by manipulating pressure distribution, delaying flow separation, and increasing effective camber or circulation around the airfoil. The primary categories of passive lift-augmentation mechanisms include **leading-edge devices**, **trailing-edge flaps**, **boundary-layer control through surface shaping**, and **high-lift airfoil design**.

4.1 Leading-Edge Devices

Leading-edge devices, such as slats, Krueger flaps, and drooped noses, are designed to increase the stall angle of attack and maintain attached flow over the upper surface at high lift coefficients. A leading-edge slat functions by forming a slot that re-energizes the boundary layer on the main wing, delaying flow separation during high angles of attack. The circulation and lift increase arise from improved pressure recovery and boundary-layer mixing. Typical lift coefficients for multi-element configurations using leading-edge slats can reach $C_L \approx 2.5–3.0$ before stall. However, their mechanical deployment and limited incremental lift relative to powered methods restrict their suitability for extreme STOL applications.

4.2 Trailing-Edge High-Lift Systems

Trailing-edge devices, including single, double, and triple-slotted flaps, increase the effective camber and chord of the wing, significantly augmenting lift during take-off and landing. Multi-element flaps exploit the pressure recovery between successive elements to achieve high lift coefficients while maintaining attached flow. For instance, a triple-slotted Fowler flap system can achieve C_L values up to 4 in clean aerodynamic conditions. Nevertheless, these systems provide diminishing returns as flap deflection increases beyond the point of flow separation. In addition, they rely entirely on aerodynamic camber effects, limiting their lift-to-drag performance in low-speed STOL regimes where flow energy addition becomes essential.

4.3 Boundary-Layer Shaping and Vortex Generators

Passive boundary-layer control methods such as vortex generators, fences, and microvanes introduce controlled streamwise vortices that enhance momentum exchange within the boundary layer. These devices delay separation and improve flow attachment, particularly on swept or highly cambered surfaces. Although they effectively improve stall characteristics and enhance controllability, their lift increment is modest ($\Delta C_L \approx 0.2–0.3$), and they introduce additional parasitic drag at cruise conditions.

4.4 High-Lift Airfoil Design

Airfoil sections specifically optimized for high-lift performance employ increased maximum camber, favorable pressure recovery characteristics, and delayed transition to turbulence. These designs, such as the NACA 230 series and NASA SC(2)-series high-lift profiles, provide inherent lift advantages without movable elements. However, the lift augmentation achieved is static and limited compared to configurations employing flow energization. Furthermore, the high camber required for passive lift enhancement often results in adverse drag penalties at cruise.

4.5 Summary of Passive Approaches

In summary, passive lift-augmentation methods enhance lift through aerodynamic shaping, boundary-layer control, and camber manipulation, but their performance is constrained by flow separation at large angles of attack. While effective for conventional take-off and landing operations, they are insufficient for achieving the high lift coefficients ($C_L > 5$) required in advanced short take-off and landing (STOL) or distributed propulsion concepts. Consequently, the present study explores **active lift-augmentation techniques**-methods that introduce additional energy or momentum into the flow-to achieve substantially higher lift performance. The various active techniques are discussed in the following section.

5 Overview of Active Lift-Augmentation Methods

Active lift-augmentation techniques are employed to increase the effective lift coefficient of an aircraft beyond that attainable by conventional high-lift devices. These methods utilize the addition of energy or momentum into the flow field to delay separation, enhance circulation, or redirect momentum. The principal active lift-augmentation concepts developed for powered-lift and short take-off and landing (STOL) aircraft include **mechanical thrust vectoring**, **upper-surface blowing (USB)**, **circulation control (CC)**, and **externally blown flaps (EBF)**. Each method operates on a distinct aerodynamic principle and presents different trade-offs in complexity, efficiency, and compatibility with distributed propulsion systems.

5.1 Mechanical Thrust Vectoring

Mechanical thrust vectoring achieves lift augmentation by physically deflecting the propulsion system or nozzle to impart a vertical component of thrust. The thrust vector is typically varied by rotating propeller pods, swiveling jet nozzles, or using movable vanes in the exhaust stream. This method can produce very high lift coefficients, particularly in vertical or short take-off configurations (e.g., the Harrier and F-35B). However, the approach introduces significant mechanical complexity, mass penalties, and control-coupling challenges. In addition, thrust vectoring violates fixed-thrust-axis constraints in conventional STOL design frameworks, making it unsuitable for applications where propulsion alignment must remain fixed.

5.2 Upper-Surface Blowing (USB)

The upper-surface blowing concept directs a high-speed jet or propeller slipstream over the upper surface of the wing, where it adheres to the contour due to the Coandă effect. The attached jet entrains ambient air and accelerates the boundary layer, delaying flow separation and increasing suction on the upper surface. USB systems, exemplified by the Boeing YC-14 and NASA QSRA, are capable of substantial lift augmentation with moderate mechanical complexity. However, they exhibit strong viscous interactions, high thermal loads in the case of jet exhausts, and complex flow curvature that

complicates analytical modeling. The sensitivity of the Coandă attachment to Reynolds number and jet temperature also limits its scalability to propeller-driven systems.

5.3 Circulation Control (CC)

Circulation control utilizes a high-velocity jet, typically ejected tangentially through a Coandă-shaped trailing-edge surface, to enhance lift by augmenting circulation around the airfoil. The continuous blowing over the curved trailing edge effectively delays separation and increases the lift coefficient without requiring large mechanical deflections. Despite its aerodynamic effectiveness, the system demands a continuous supply of high-pressure air, complex internal ducting, and precise flow control, leading to significant penalties in system integration, weight, and energy efficiency-particularly in electrically powered aircraft architectures.

5.4 Externally Blown Flap (EBF)

In the externally blown flap configuration, the propeller or fan slipstream impinges directly on a deflected flap located downstream of the propeller disk. The slipstream is turned downward by the flap, generating lift through the vertical projection of the deflected momentum and by increasing the dynamic pressure on the wing's aft sections. The EBF concept provides lift augmentation primarily through aerodynamic momentum redirection rather than mechanical vectoring, making it inherently compatible with fixed-thrust-axis constraints. Historically, this mechanism has demonstrated excellent performance in aircraft such as the Breguet 941 and the Doak VZ-4, achieving lift coefficients exceeding five while maintaining attached flow at large flap deflections.

6 Justification for Using EBF Concept with DEP

Based on the objectives outlined in the problem statement, the present design adopts an **Externally Blown Flap (EBF)** configuration integrated with **Distributed Electric Propulsion (DEP)**. This combination enables significant lift augmentation through aerodynamic deflection of propeller slipstreams while maintaining a fixed-wing layout and avoiding the mechanical complexity of thrust vectoring or tilt mechanisms.

6.1 Physical Basis of the Externally Blown Flap Mechanism

In the externally blown flap concept, the propeller slipstream passes directly over the wing trailing-edge region and impinges on a deflected flap. The high-momentum slipstream is turned downward by the flap, thereby generating an additional lift component through the vertical projection of the deflected momentum and by increasing the effective dynamic pressure on the flap and aft wing sections. The total lift increment may be expressed as

$$\Delta L = \dot{m}(V_2 \sin\theta - V_\infty \sin\alpha), \tag{1}$$

where $\dot{m}$ is the mass flow through the propeller disk, θ is the slipstream turning angle, and α is the angle of attack. This mechanism enhances lift both by direct momentum deflection and by augmenting the circulation on the aft portion of the wing.
Because the slipstream remains attached and energized over the flap surface, the externally blown configuration delays separation at high flap deflections, enabling high lift coefficients ($C_L > 5$) without flow detachment-behavior consistent with historical STOL aircraft such as the Breguet 941 and NASA QSRA.

6.2 Advantages of Externally Blown Flaps with Distributed Propulsion

The use of distributed electric propulsion (DEP) significantly amplifies the aerodynamic benefits of the externally blown flap concept. Multiple small-diameter propellers positioned along the wing span generate overlapping slipstreams that uniformly energize the boundary layer, producing a quasi-continuous distribution of high-momentum flow over the flap. This provides several key advantages:

- **Enhanced lift augmentation:** The distributed slipstreams increase the effective dynamic pressure over a larger spanwise extent of the wing, reducing spanwise lift gradients and improving overall lift effectiveness.
- **Boundary-layer re-energization:** Continuous propeller slipstreams prevent flow separation at high flap deflections by maintaining attached flow and increasing local Reynolds number, thus extending the linear lift regime.
- **Improved control authority and redundancy:** DEP enables fine-grained thrust modulation across the span, offering differential thrust control for pitch, roll, and yaw moments without the need for mechanical vectoring surfaces.
- **System integration:** Electrically driven propellers allow for compact nacelle design, reduced mechanical complexity, and flexible placement close to the wing surface-conditions favorable for maximizing slipstream–flap interaction efficiency.

Furthermore, the EBF-DEP configuration avoids the high thermal loads and viscous jet–surface interactions characteristic of upper-surface blowing (USB) and the mechanical complexity of thrust-vectoring systems. It retains the core advantage of powered lift through aerodynamic momentum redirection while remaining mechanically simple and energy-efficient within the distributed electric propulsion framework.
The EBF–DEP architecture therefore represents the optimal compromise between aerodynamic performance and system integration. It provides the lift augmentation benefits of a powered-lift system without violating non–thrust-vectoring constraints, while remaining compatible with distributed electric propulsion and scalable for various wing spans and power loadings.

7 Theoretical Models for EBF Systems

This section details the theoretical models used to analyze the Propeller Blown Wing / Externally Blown Flap (EBF) configuration. The analysis begins with foundational analytical and semi-empirical formulations and transitions to the modern non-dimensional parameters used for computational analysis.

7.1 Foundational Analytical and Semi-Empirical Models

A number of analytical and semi-empirical formulations have been developed to predict the aerodynamic characteristics of EBF configurations. These models attempt to represent the complex aerodynamic interaction between the propeller slipstream, the wing, and the deflected flap using simplified physical assumptions.

7.1.1 Simple Momentum Theory Models

The earliest mathematical representations of EBF aerodynamics were based directly on momentum theory. The propeller slipstream is treated as a jet with uniform velocity V_s and mass flow rate $\dot{m}$, which impinges on a flap and is deflected by an angle θ. The resulting change in vertical momentum produces an incremental lift force:

$$\Delta L = \dot{m}(V_s \sin\theta - V_\infty \sin\alpha), \tag{2}$$

while the longitudinal force (drag) increment is

$$\Delta D = \dot{m}(V_\infty \cos\alpha - V_s \cos\theta). \tag{3}$$

This formulation, sometimes referred to as the *deflected slipstream model*, provides first-order estimates but neglects aerodynamic coupling and pressure distribution changes.

7.1.2 Spence's Jet Flap Theory

To capture the circulation augmentation produced by the slipstream, Spence's Linear Jet Flap Theory [1] provides a baseline 2D estimate. This model predicts the sectional lift coefficient (c_l) as a function of angle of attack (α), flap deflection (δ_F), and jet momentum (c_J).

- **Combined Lift Formula:**

$$c_l = \frac{\partial c_l}{\partial \alpha}\alpha + \frac{\partial c_l}{\partial \delta_F}\delta_F \tag{4}$$

- **Lift-Curve Slope (Effect of α):**

$$\frac{\partial c_l}{\partial \alpha} = 2\pi(1 + 0.151\sqrt{c_J} + 0.219 c_J) \tag{5}$$

- **Flap Effectiveness (Effect of δ_F):**

$$\frac{\partial c_l}{\partial \delta_F} = 2\sqrt{\pi c_J}(1 + 0.151\sqrt{c_J} + 0.139 c_J)^{\frac{1}{2}} \tag{6}$$

Note: This linear theory tends to over-predict lift as it assumes 100% efficient flow turning, but it serves as a foundational theoretical model for circulation-enhanced flow [2].

7.1.3 Jet-Turning Control-Volume Models (Sforza, 1966)

Sforza introduced a more comprehensive control-volume model by explicitly evaluating the turning of the slipstream [3]. The approach considers the conservation of mass, momentum, and energy. The lift and drag coefficients are expressed as:

$$C_L = C_{L,\text{off}} + \frac{2T}{\rho V_\infty^2 S} \sin(\theta + \alpha), \tag{7}$$

$$C_D = C_{D,\text{off}} + \frac{2T}{\rho V_\infty^2 S}(1 - \cos(\theta + \alpha)), \tag{8}$$

where T is the total propeller thrust. This formulation connects the lift increment to thrust and turning angle but neglects viscous losses.

7.1.4 Brown and Michael (1961) Semi-Empirical Model

Brown and Michael proposed a semi-empirical model that separates the lift contribution into pressure-induced and momentum-induced components [4]. The incremental lift coefficient is given by:

$$\Delta C_L = \frac{2C_T'}{S/S_p} \sin(\theta + \alpha) + \beta \frac{S_p}{S} \left(\frac{V_s}{V_\infty} - 1 \right), \tag{9}$$

where C_T' is the nondimensional thrust coefficient, S_p the propeller disk area, and β an empirical coupling parameter.

7.1.5 Kuhn's Semi-Empirical Model (1959)

The present study uses the semi-empirical model developed by Richard E Kuhn of NASA Langley Research Center. Below, we present a theoretical background of the Model and justify our rationale for selecting it to model our powered wing design.

Aerodynamic modelling of powered or blown wings requires capturing the coupled effects of the propeller slipstream, lifting surface, and high-lift devices with computational efficiency. The semi-empirical method of Richard E. Kuhn [5] provides an optimal balance of accuracy and efficiency, using momentum theory with empirical corrections to predict lift and longitudinal forces in deflected-slipstream conditions.

Physical Relevance and Underlying Theory

Kuhn's method models the total aerodynamic forces as the sum of contributions from three distinct flow components:

1. the conventional power-off wing,
2. the direct lift generated by thrust deflection, and
3. the incremental lift arising from increased mass flow through the slipstream.

Kuhn's method represents a major advancement in EBF modeling by combining the momentum-balance approach with empirical correction factors derived from extensive NASA and NACA experimental data. The governing equation for the lift coefficient is expressed as:

$$C_L = C_{L,\text{off}} + F_T C_T' \sin(\theta + \alpha) + k F_T C_T' \sin(\theta + \alpha) \left(1 + \frac{C_T' S}{N S_p}\right)^{-1/2} \tag{10}$$

where F_T is the thrust recovery factor, k an empirically determined constant (typically $k \approx 1.8$), N the number of propellers, and other symbols retain their previous meanings. This method captures both the direct thrust deflection and the mass-flow increase effects, providing accurate lift predictions (within 10% of experimental data) across a wide range of flap deflections and thrust coefficients. Kuhn's model remains the standard semi-empirical reference for deflected-slipstream systems.

Validation and Applicability to the Present Configuration

Kuhn's method has been extensively validated for propeller-driven short take-off and landing (STOL) aircraft, notably the *Breguet 941*, which features large-chord triple-slotted flaps positioned within the slipstream of four turboprop engines. The semi-empirical predictions demonstrated less than 10% deviation in lift coefficients when compared with both wind-tunnel and flight data up to the onset of stall. Similar validation against CFD simulations for the NASA *X-57 Maxwell* distributed electric propulsion configuration further confirmed the robustness of the approach for modern distributed-propulsion systems.

Given that the present powered wing concept exhibits a comparable aerodynamic mechanism-lift enhancement through propeller slipstream deflection over a high-lift flap system-Kuhn's method provides a reliable means to predict performance across a wide range of thrust coefficients, flap deflections, and propeller geometries.

Computational Efficiency and Suitability for Conceptual Design

High-fidelity CFD or vortex-lattice coupling methods, though accurate, are computationally prohibitive for conceptual design iterations. Kuhn's framework, being semi-empirical, requires only basic geometric and thrust parameters (c_f/D, δ_f, C_T', θ, F_T) to yield rapid estimations of C_L and C_D.

This allows efficient trade-off analysis between propeller placement, flap sizing, and distributed thrust levels-an essential requirement in early-stage design of powered-wing systems.
The semi-empirical formulation proposed by Kuhn has been widely adopted in preliminary aircraft design tools for the estimation of powered-lift aerodynamic characteristics. It has also been successfully implemented in professional aircraft design environments such as the Onera–Airbus–Dassault (OAD) Aircraft Design Software (ADS), demonstrating its suitability for integration within conceptual design frameworks.

Known Limitations and Controlled Assumptions

Kuhn's method assumes fully developed slipstream at the wing and neglects swirl-induced spanwise flow effects. It is valid primarily in the unstalled regime, where the flow remains attached over the flaps. Despite these simplifications, the method accurately reproduces key aerodynamic trends, including:

- the linear increase of C_L with thrust coefficient up to stall,
- the shift in effective lift curve slope due to slipstream momentum addition, and
- the degradation of longitudinal force prediction at very high deflections.

These limitations are well characterized and manageable within the design space of the current study.

8 Hyperparameter Study

The primary goal is to find a single, optimal design configuration from a set of discrete variables. The "best" configuration is defined by:

- **Primary Objective:** Maximizing a key performance metric (e.g., Lift Coefficient, C_L).
- **Performance Constraints:** Simultaneously satisfying a set of minimum thresholds (e.g., $C_L > C_{L,min}$ and Lift-to-Drag Ratio $L/D > (L/D)_{min}$).

8.1 Model and Data Preparation

The evaluation of each design point relies on a core computational model.

1. **Evaluation Model:** A semi-empirical formula (e.g., Kuhn's method) is used to calculate the primary outputs (C_N, C_X) from a set of inputs.
2. **Data Loading:** The model is fed with baseline data loaded from external files:
    - **Power-Off Aerodynamics:** Airfoil polar data is loaded to provide baseline $C_{L,off}$ and $C_{D,off}$ values as a function of Angle of Attack (α).
    - **Empirical Relationships:** Digitized experimental data (e.g., turning_angle.csv) is loaded to provide interpolation functions for key model parameters, such as slipstream turning angle (θ) and its physical limits (θmax).

8.2 Parameter Space Definition

The "hyperparameter" study is defined by iterating over a discrete set of values for several independent design variables. The total number of simulations is the product of the number of options for each variable.

Table 1: Example 5-Dimensional Design Space

Parameter	Symbol	Discretized Values
Aspect Ratio	AR	$\{8, 9, 10\}$
Number of Propellers	N	$\{4, 6, 8\}$
Angle of Attack	α	$\{4.0, 6.0\}$ deg
Flap Chord	c_f	$\{0.08, 0.10, 0.12, 0.14\}$ m
Flap Deflection	δ_f	$\{30, 40, 50, 60\}$ deg

8.3 Execution Strategy: Brute-Force Sweep

A **grid search** (or brute-force) methodology is employed by constructing a series of 5 nested `for` loops. The execution flows from the outermost loop (e.g., Aspect Ratio) to the innermost (e.g., Flap Deflection).

8.4 Evaluation and Filtering

For each of the (e.g., 432) combinations, a multi-step evaluation and filtering process is applied:

1. **Calculate Derived Geometry:** Inside the loops, key geometric properties are calculated (e.g., $b = \sqrt{AR \cdot S_w}, c_w = S_w/b, D = b/N$).

2. **Geometric Constraint Check:** A "hard" constraint is applied to check for geometric realism. For example:

   $$\text{if } 0.20 \leq (c_f/c_w) \leq 0.35 : \text{ proceed}$$

   If the check fails, the configuration is discarded, and the innermost loops are skipped.

3. **Run Evaluation Model:** The valid configuration is passed to the computational model.

   - The model interpolates to find $C_{L,off}$ and $C_{D,off}$ for the given α.
   - It calculates the total turning angle $\theta_{total} = \theta_w + \theta_f$.

4. **Physical Constraint Check:** A "soft" constraint is applied to check for physical validity.

   $$\text{if } \theta_{total} \leq \theta_{max} : \text{ proceed}$$

If the flow is stalled ($\theta_{total} > \theta_{max}$), the configuration is flagged as "FAILED (Theta Limit)" and discarded.

5. **Calculate Final Metrics:** For valid configurations, the final body-axis forces (C_N, C_X) and the final performance metrics (C_L, C_D, L/D) are calculated using their respective formulae.
6. **Store Results:** All calculated inputs and outputs for the valid run are stored.

8.5 Optimal Candidate Selection

After the simulation sweep is complete, the set of all valid, non-failed results is processed to find the "best" configuration.

1. **Filter by Performance:** The results are filtered to find the subset of "successful" candidates that meet all performance targets:

$$\text{Candidates} = \{\text{run} \mid \text{run}[C_L] > 6.5 \text{ AND run}[L/D] > 5.0\}$$

2. **Select Best:** The "best" configuration is selected from this successful subset by applying the primary objective:

$$\text{Best} = \max_{\text{Candidates}} (\text{run}[C_L])$$

3. **Report:** A detailed report of the single best configuration is printed, showing all of its input parameters and resulting performance metrics. If no configuration meets the targets, a failure message is reported.

9 Wing Design Methodology

To design the wing based on Kuhn's method, we came up with the following methodology:

1. Choose a high-lift airfoil (choice in section 8.1).
2. Fix a lift coefficient C_L.
3. Parameterise all unknowns in terms of the chord length c_w.
4. Solve the governing equation for the lift equation (equation 10) to obtain c_w, D, S.
5. Based on the D obtained, we decide the propeller as mentioned in subsection 8.2 below.

The goal is to fix a few parameters that we can work with. The lift coefficient equation is modified in terms of another parameter - the wing chord length c_w.

Parameters Fixed

- N - Number of propellers along wingspan
- AR - Aspect ratio of the wing
- B - A constant between 0 and 1 that gives flap chord length by $c_f = Bc_w$
- α - Angle of attack
- θ - Total turning angle of the slipstream

The first equation we obtain is for the flap angle δ_f. This is derived from the total turning angle equation, given by

$$\theta = \theta_w + \theta_f \tag{11}$$

where θ_w and θ_f depend on the airfoil geometry. θ_w and θ_f can be determined from experimental graphs that relate them to c_w, c_f, and D(Propeller diameter). Hence, the flap deflection angle can be expressed as

$$\delta_f = \frac{\theta - (\frac{\theta}{\delta})_w \delta_e}{(\frac{\theta}{\delta})_f}$$

δ is the turn angle per degree of flap/wing angle respectively

Lift Coefficient Equation

We now move on to the lift coefficient equation, expressed as

$$C_L = C_{L,\text{off}} + \frac{F}{T} C_T' \sin(\theta + \alpha) + k \frac{F}{T} C_T' \sin(\theta + \alpha) \frac{1}{\sqrt{1 + \frac{C_T' S}{N S_p}}} \tag{12}$$

where $C_{L,\text{off}}$ is the power-off lift coefficient, C_T' is the total thrust coefficient, and $k = 1.8$ is a correction constant (based on Kuhn's empirical correction).
We must rewrite this in terms of c_w, the wing chord length.

Intermediate Relations

The total thrust is given by

$$NT = \text{Total Thrust (known quantity)}$$

The dynamic pressure is

$$q = \frac{1}{2} \rho V^2$$

and the wing surface area is

$$S = \text{wingspan} \times \text{wing chord length} = b\, c_w = (AR)\, c_w^2$$

Thus, the total thrust coefficient becomes

$$C_T' = \frac{T_{tot}}{q(AR)c_w^2}$$

We are assuming that the entire wingspan is covered by N propellers, each of diameter D, such that

$$ND = \text{wingspan} \quad \Rightarrow \quad D = \frac{AR\, c_w}{N}$$

and the propeller disc area is

$$S_p = \frac{\pi D^2}{4} = \frac{\pi (AR)^2 c_w^2}{4N^2}$$

Modified Expression for C_L

Substituting the above relations, the lift coefficient can be rewritten as

$$C_L = C_{L,\text{off}} + \frac{F}{T} \cdot \frac{T_{tot}}{q(AR)c_w^2} \sin(\theta + \alpha)\left(1 + \frac{k}{\sqrt{1 + \frac{4T_{tot}N}{q\pi (AR)^2 c_w^2}}}\right) \tag{13}$$

or equivalently,

$$c_w^2 = \frac{T_{tot} \sin(\theta + \alpha)}{q(AR)(C_L - C_{L,off})}\left(1 + \frac{k}{\sqrt{1 + \frac{4T_{tot}N}{q\pi (AR)^2 c_w^2}}}\right) \tag{14}$$

This equation allows the target lift coefficient C_L to be specified, and the corresponding value of c_w to be determined. This equation is solved numerically because we cannot rearrange this equation to obtain an explicit equation for c_w

Rearranged Form

Defining

$$\gamma = \frac{T_{tot} \sin(\theta + \alpha)}{q(AR)(C_L - C_{L,off})}, \psi = k, \mu = \frac{4T_{tot}N}{q\pi (AR)^2}$$

the equation can be rewritten compactly as

$$c_w^2 = \gamma\left(1 + \frac{\psi}{\sqrt{1 + \frac{\mu}{x^2}}}\right) \tag{15}$$

From this relation, c_w can be obtained for a target lift coefficient C_L. Using the previously defined relations, all other unknowns can be subsequently computed.

It is important to ensure that θ_w and θ_f are both less than their maximum allowable values $\theta_{w,\max}$ and $\theta_{f,\max}$, so that no stalling occurs during operation.

9.1 Choice of Airfoil geometry

For testing our theory, we used the Eppler E423 high-lift airfoil due to its high camber, which generates significant upward lift.

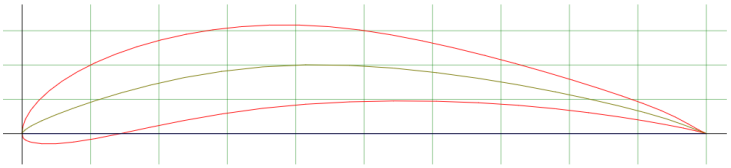

Figure 1: E423 Airfoil

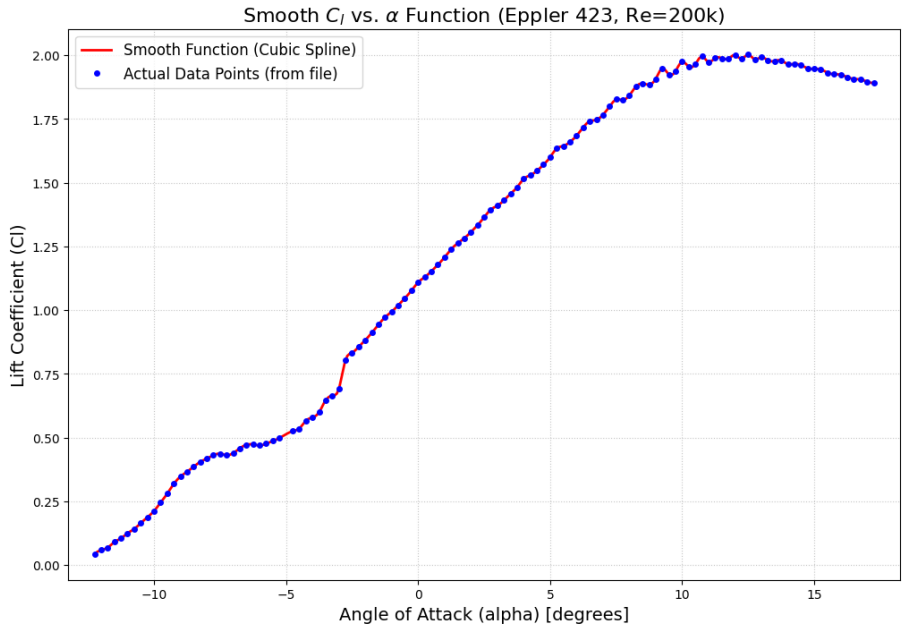

Figure 2: C_L Vs α

9.2 Choice of Propeller

The specified C_L is a theoretical value. After we get c_w, we choose a desired propeller satisfying the diameter and thrust requirements. Using the available data on that propeller, we recalculate the real lift coefficient.

The data for the propellers was obtained from Advanced Precision Composites (APC) propellers. Their website has an extensive for different configurations of propellers.

Nomenclature: As stated in the APC propeller nomenclature, the size of each propeller is identified by two numbers separated by an 'X'. The first number indicates the diameter of the propeller in inches and the second number indicates the pitch of the propeller in inches. The letter after the second number indicates the type of the propeller ('E' for electric, only letter relevant to our use case).
For example, consider the propeller 'PER3_13X7E'. This implies that the diameter of the propeller is 13 in, its pitch is 7 in and it is an electric propeller.

A script was written which goes through the database of all the propellers, and based on the D obtained from the calculation of c_w, we find the propeller with the corresponding diameter and an operational velocity of 20 m/s, which is around 45 mph. In case an exact value corresponding to the velocity is not present, we perform linear interpolation to obtain that value, and as a result we get the required value at 20 m/s.
Note: All propellers in the database are two-bladed. For considering three-bladed or four-bladed propellers, a simple modification can be made to the data. The conversion is made by matching the two-blade torque for the specified model speed and RPM conditions. Multiply D by 0.9 (for three-blades) or 0.84 (for four-blades) to convert the propeller.

From this method, we find out the operational RPM and the thrust generated by the propeller. A propeller can be considered a successful candidate if:

1. The product of the number of propellers and the thrust from a single propeller lies within the given thrust envelope.
2. The operational RPM of the propeller is less than or equal to 150000/D.
3. The total drag generated by all the propellers combined small enough such that it is above the given lift-to-drag ratio.

9.3 A Preliminary calculation

Now, let us look at a preliminary calculation based on the above described method. We will be using the E423 airfoil at an angle of attack $\alpha = 12°$ so that $C_{L,off}$ is nearly at its maximum. We choose $C_{L,off} = 1.98$. Since the other initializing variables can be treated as hyperparameters, we can choose any values for these, provided they produce results within the domain and are within the individual limits of each variable. Therefore we fix the following:

$$
\begin{aligned}
N &= 6 \\
AR &= 10 \\
B &= 0.12 \\
\alpha &= 12^\circ \\
\theta &= 60^\circ \\
T_{tot} &= 96N \text{(Taking the higher end of the thrust envelope)} \\
C_L &= 8 \text{(Target Lift coefficient)} \\
\rho &= 1.225 \text{kg/m}^3 \\
v &= 20 \text{ m/s}
\end{aligned}
$$

Now from all these parameters, we find the constants $\gamma, \psi, \& \mu$.

$$
\begin{aligned}
\gamma &= \frac{T_{tot} \sin(\theta + \alpha)}{q(AR)(C_L - C_{L,off})} = 0.00619 \\
\psi &= k = 1.8 \\
\mu &= \frac{4T_{tot}N}{q\pi(AR)^2} = 0.02993
\end{aligned}
$$

Substituting these values into equation(15), we get $c_w = 0.11m$. Now from this value we get all the other required information:

$$
\begin{aligned}
S &= 0.121m^2 \text{(Wing Surface Area)} \\
WS &= 0.11m \text{(Wingspan)} \\
D &= 0.018m \text{(Propeller diameter)}
\end{aligned}
$$

Now, we visit the propeller database and choose a propeller of the same diameter, and find the the rpm at which the thrust produced by these propellers is within our thrust envelope for the given takeoff speed of 20 m/s. We chose the propeller with a diameter of 17.78 cm from the database (closest to our calculated value), and got the operational RPM of the propeller at which enough thrust was being produced to be within our required thrust envelope. From the data, we got an approximate thrust of 13.342 N per propeller, with the thrust plant producing 6 times the thrust per propeller of 80.052 N. Substituting this value of T_{tot} into equation(10), we get an effective lift coefficient of $C_L = 7.76$. This is close to the $C_L = 8$ that we gave the model to calculate c_w. Therefore, this preliminary calculation

shows us that the estimated lift by using data is also quite close to the target lift coefficient.
Substituting these data values into the Kuhn's equation, we get an approximate lift coefficient $C_L = 7.76$ and thrust per propeller to be $13.342N$. So 6 propellers would produce a total thrust of 80.052 N.

10 CFD Methodologies/Strategies Explored

We explored the findings of this paper, "Selection of Propeller-Wing Configuration on Blown Wing Aircraft", to establish a robust and computationally feasible methodology for our own preliminary CFD analysis. The paper's authors faced a similar challenge: exploring a vast design space where full-fidelity, transient simulations of all configurations are computationally prohibitive. Their systematic validation of simplified models provides a clear and rigorous blueprint for our approach.
This following section of the report details the theoretical foundations, key assumptions, and procedural steps, as derived from the paper, that justify our use of a 3D/2D, steady-state actuator disk model with a uniform pressure rise (no swirl)

10.1 Theoretical Foundation

Any valid Computational Fluid Dynamics simulation of this problem statement must capture the two essential physical phenomena that govern the performance of a blown wing:

1. The mechanism of Lift Augmentation
2. The unique Mechanism of stall

10.1.1 Primary Aerodynamic Principle: Lift Augmentation

The fundamental benefit of a blown wing is the "Blowing" of the wing with the high velocty propellor jet, which increases the dynamic pressure over the airfoil. The paper presents the theoretical relationship for the augmented lift coefficient (Clblown) for an infinitely large jet as:

$$C_{L,blown} = C_{L,unblown} \frac{V_j^2}{{V_\infty}^2} \tag{16}$$

This equation dictates that the augmented lift scales with the square of the jet velocity (V_j) relative to the freestream velocity (V_∞). For a fixed thrust, a smaller jet area results in a higher V_j, theoretically offering a path to exceptionally high lift coefficients. Our CFD model must, at a minimum, be able to capture this fundamental addition of energy and its effect on lift.

10.1.2 Stall Mechanism

The paper's most critical insight is its identification of the stall mechanism. This is not a traditional high-angle-of-attack flow separation. Instead, it is a sudden and catastrophic loss of lift that occurs when the wing, due to a change in angle of attack or flap angle, moves outside the propeller's jet.

1. **Mechanism**: When the jet passes just above the wing's upper surface, it causes a "sudden rise in diffusion on the rear of the suction surface" , which in practice results in boundary layer separation and stall. The paper quantifies this using a Diffusion Factor (DF) in Figure 8:

$$DF = \frac{V_{peak} - V_{TE}}{V_{\infty}}$$

This stall is therefore a geometrically-driven event. The paper explicitly confirms this: "It can be seen that the stall condition, in all three cases, occurs at the point where the jet just moves above the wing". To avoid this, the paper presents a simple geometric inequality that must be satisfied:

$$\frac{D_p}{2} - y_p \geq f(x_p)$$

where y_p is the propeller's vertical position and $f(x_p)$ is the stagnation streamline coordinate.

2. **Implication**: Therefore, our model's primary requirement is not necessarily to capture the fine-scale turbulence of rotation, but to accurately predict the jet's trajectory, height, and interaction with the wing's upper surface, as this is what dictates the operational stall boundary.

11 Comparison of CFD Model Fidelities

The reference paper, "Selection of Propeller-Wing Configuration on Blown Wing Aircraft," validates its primary 2D methodology by first comparing three models of increasing complexity. This comparison is essential for understanding the trade-offs between computational cost and physical accuracy.

11.1 Description of the Models

The three models investigated by the authors are (as shown in Fig. 3):

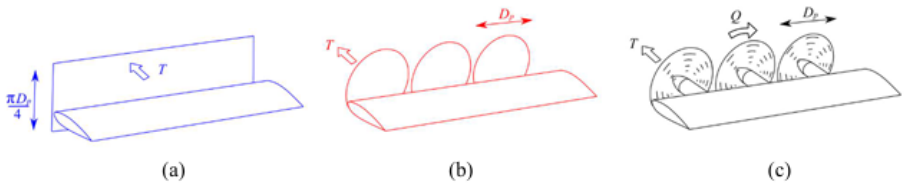

Figure 2. Levels of model fidelity, (a) 2D actuator disc with uniform pressure rise, (b) 3D actuator disc with uniform pressure rise, (c) 3D actuator disc with radial work profile and exit swirl.

Figure 3: Different Models used for simplifying CFD simulations as per referred paper.

Case A: 2D Actuator Disc This is a 2D simulation using an actuator disc with a uniform pressure rise. It represents the highest level of simplification, reducing the problem to a two-dimensional slice.

Case B: 3D Actuator Disc (Uniform Pressure Rise) This model advances to 3D, modeling a 3D actuator disc with a uniform pressure rise. This case correctly captures the three-dimensional geometry of the wing and the spanwise non-uniformity of the jet's height but **omits the rotational effects (swirl)** of the propeller.

Case C: 3D Actuator Disc (Swirl & Radial Profile) This is the highest-fidelity model used in the validation, modeling a 3D actuator disc with a non-uniform radial work profile and exit swirl. This case simulates the tangential forces (F_θ) applied to the fluid, which are generated by a rotating propeller.

11.2 Key Findings from the Model Comparison

By comparing these three cases, the authors were able to isolate the physical impact of 3D geometry and rotational swirl. The results (shown in Fig. 4) are the cornerstone of our methodological justification:

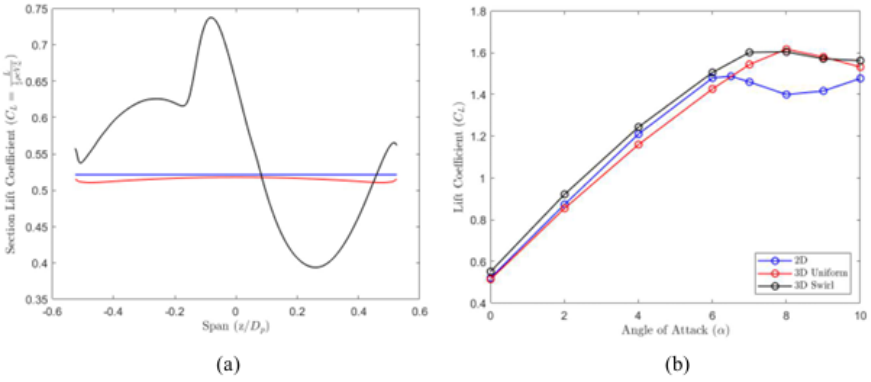

Figure 3: (a) Spanwise lift distribution, (b) Coefficient of lift plotted against angle of attack

Figure 4: Comparison of the three simulation Cases.

- **Effect of 3D Geometry (Case A vs. B):** The spanwise non-uniformity in jet height (present in 3D but not 2D) was found to have "little effect on the spanwise loading" and only a "second order effect on the lift distribution", provided the wing remains submerged in the jet.
- **Effect of Swirl (Case B vs. C):** The introduction of swirl (Case C) "has a significant effect on the spanwise lift distribution". This is visually evident in the non-uniform '3D Swirl' line in Fig. 3a.
- **Impact on Key Performance Metrics (The Critical Finding):** Despite the significant change in spanwise load distribution, the paper explicitly states that the introduction of swirl "was found to have **only a second order effect** on the gradient of the lift coefficient with angle of attack and on the angle of attack at which stall occurs".
- **Maximum Lift Agreement:** Across all three models, from the simplest 2D to the most complex 3D with swirl, the "maximum lift agrees to within 7%".

12 Justification for Our Two-Stage Methodology

Based on the paper's clear findings, we have adopted a two-stage methodology. This approach allows us to leverage the speed of simplified models for broad exploration and the accuracy of higher-fidelity models for validation, all while avoiding unnecessary computational expense.

12.1 Stage 1: 2D Actuator Disc Analysis

Our first step is to replicate the paper's primary method: a broad parameter-space study using the 2D actuator disc model (Case A).

- **Purpose:** To rapidly explore the configuration space (i.e., vary propeller diameter D_p, vertical position y_p, and axial position x_p).
- **Justification:** The paper's authors chose this approach precisely because the "simplification of modelling the blown wing in only two-dimensions added a simplicity to the problem that allowed a clearer understanding of the configuration space". This 2D model is computationally inexpensive, allowing for hundreds of simulations to identify regions of high performance and understand the first-order sensitivities.

12.2 Stage 2: 3D Uniform Pressure-Rise Analysis

Once the 2D study identifies a set of promising configurations, we will advance to a higher-fidelity 3D simulation using the "3D Uniform" model (Case B).

- **Purpose:** To validate the 2D findings and obtain more accurate, three-dimensional performance data for the optimal designs, without the extreme cost of a full swirl simulation.
- **Justification:** This model is the perfect balance of accuracy and cost, for the following reasons:
    1. **It Captures 3D Effects:** Unlike the 2D model, this model correctly captures the 3D geometry of the wing and the 3D shape of the propeller jet.
    2. **It Is Computationally Cheaper than Swirl:** It omits the rotational physics of swirl ($F_\theta = 0$).
    3. **It Is Validated by the Paper:** The paper *explicitly proved* that omitting swirl (i.e., using Case B instead of Case C) has only a "second order effect" on the key metrics we care about: the stall angle and the lift coefficient gradient. The maximum lift also remains accurate to within 7%.

12.3 Conclusion

This two-stage approach is directly supported by the paper's own findings. The 2D model provides the necessary speed for a broad design exploration, while the 3D uniform-pressure model provides a

high-fidelity validation step that captures 3D geometric effects. Critically, we can confidently use this 3D model without swirl, as the paper demonstrates that rotational effects are of secondary importance to the primary performance metrics for this specific problem.

13 CFD Procedure

13.1 Geometry and Model Description

For preliminary exploration, a three-dimensional (**3D**) wing model based on the **NACA 4412 airfoil** was created in **Autodesk Fusion 360**. This initial setup was intended to study general flow behaviour and understand how the propeller-induced flow interacts with the wing surface. The geometry was refined in **ANSYS Discovery** to ensure it was watertight and suitable for CFD.
However, the 3D simulation proved to be highly **computationally expensive** and time-consuming, particularly during meshing and solver setup in SimScale. After gathering the required aerodynamic details such as the actual airfoil type (**Eppler E423**), chord length, and propeller diameter, the study was continued using a simplified **two-dimensional (2D)** geometry. This 2D model represented a thin section of the wing, chosen to reduce computational cost while still capturing essential aerodynamic characteristics.

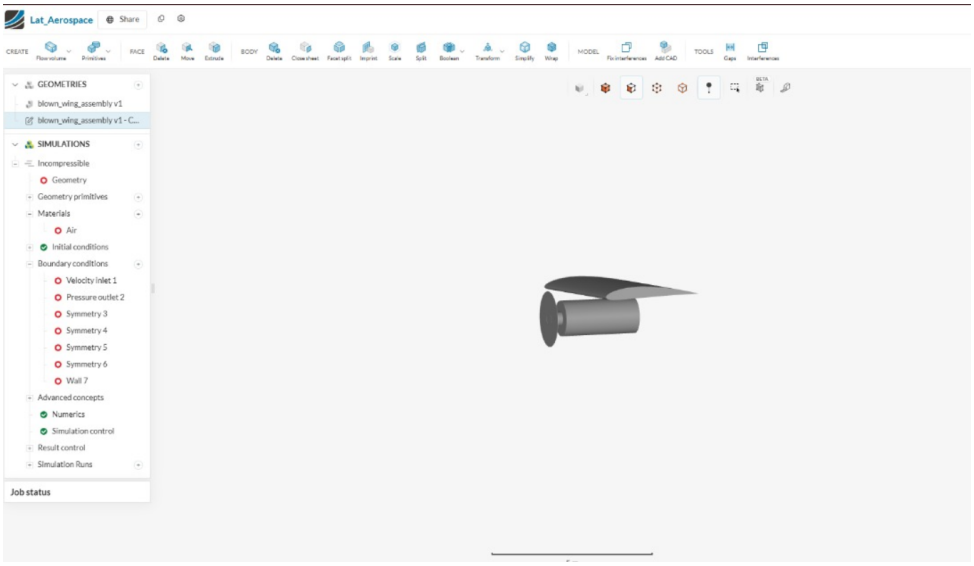

Figure 5: 3D model based on NACA 4412 airfoil created for preliminary flow exploration.

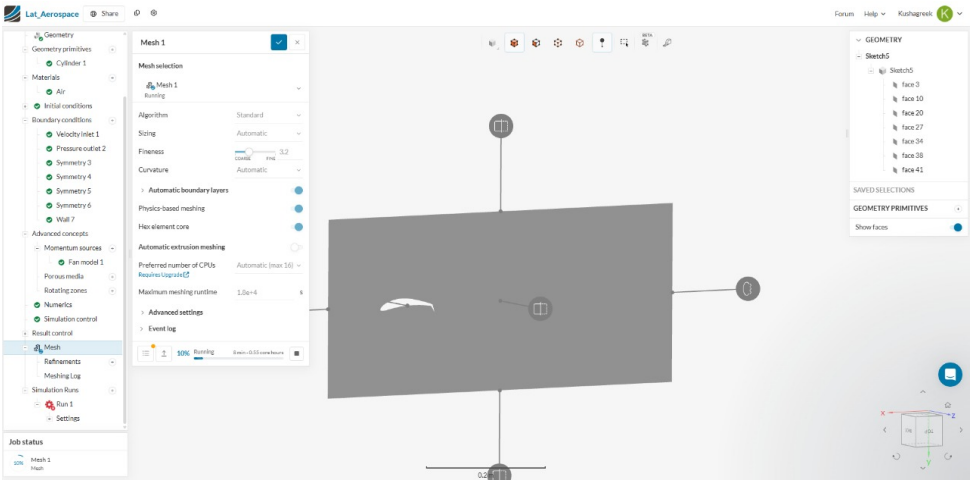

Figure 6: 2D model of the E423 wing section with defined flow domain in SimScale.

13.2 Computational Domain and Boundary Conditions

The computational domain for both the 3D and 2D setups was created in **SimScale**. The boundaries were placed far enough from the geometry to minimize blockage effects and ensure stable inflow and outflow conditions.

The boundary conditions were defined as follows:

- **Inlet:** Uniform velocity inlet of 20 m/s in the $+x$ direction.
- **Outlet:** Pressure outlet with a gauge pressure of 0 Pa.
- **Top, bottom, and side walls:** Treated as symmetry or velocity inlets to represent far-field flow.
- **Wing and disk surfaces:** Assigned as no-slip walls.

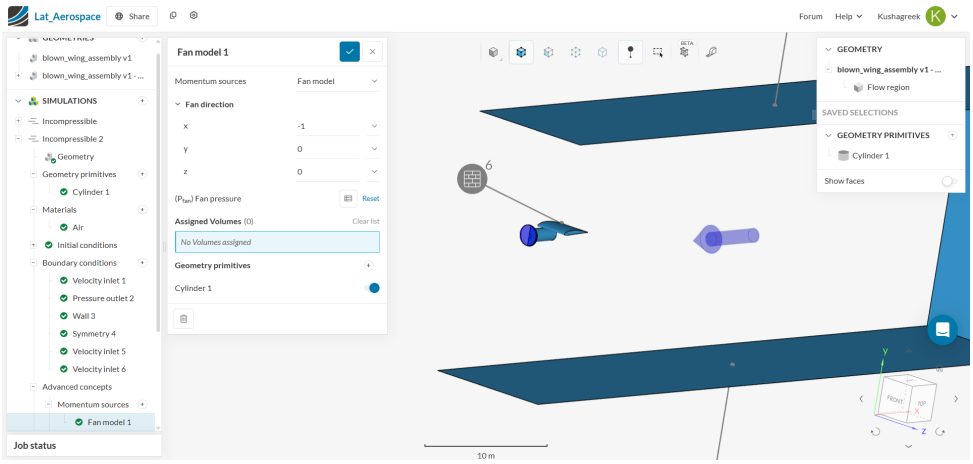

Figure 7: Momentum source term added in place of the propellor as a cylindrical primitive to simulate blown wing effect.

In the 3D case (without swirl), the propeller effect was represented by a **momentum source** using SimScale's *fan model*, aligned with the x-axis. This approach approximates the induced velocity caused by the propeller while significantly reducing computational requirements.

13.3 Mesh Generation and Future Work

A **hex-dominant mesh** using **physics-based meshing** was planned in SimScale. Refinements were applied around the leading and trailing edges of the wing, the actuator disk region, and the wake zone, with prism layers on the wing surface to resolve boundary-layer development accurately.
However, even for the 2D configuration, the meshing process required a long computation time in SimScale and could not be completed within the current project period. Due to these time constraints, the full CFD simulation could not be performed.
The complete meshing and simulation will be carried out during the **end-term phase**. The final model will include the **actual propeller geometry**, allowing for accurate determination of both the **lift (C_L)** and **drag (C_D)** coefficients and a more realistic assessment of the aerodynamic performance of the wing–propeller configuration.

14 Targets for end term

The next phase of this project will focus on translating the theoretical framework and preliminary modeling efforts into high-fidelity numerical validation and optimized design refinement. The following key tasks are planned for the end-term stage:

Completion of CFD Mesh Generation and Simulation Runs

The meshing process initiated in the mid-term stage will be finalized using a high-resolution, hex-dominant mesh with refined boundary-layer treatment. Steady-state simulations will be performed for multiple configurations of propeller placement, flap deflection, and angle of attack to quantify their influence on lift augmentation. The lift and drag coefficients obtained will be compared against the theoretical predictions from Kuhn's semi-empirical model.

Parametric Sensitivity Analysis

A systematic study will be conducted to evaluate the sensitivity of aerodynamic performance to key design variables such as propeller diameter, spacing, and flap deflection angle. This analysis will help identify the optimal configuration that maximizes lift while maintaining favorable lift-to-drag ratios and acceptable power requirements.

3D CFD Validation and Comparison

Building on the two-stage methodology, a detailed 3D simulation incorporating a uniform pressure-rise actuator disk model will be carried out to validate the 2D findings. The 3D results will be used to assess spanwise flow effects, induced drag variation, and slipstream–flap interactions, providing a more complete aerodynamic characterization of the powered-lift wing.

Investigation of Flow Separation and Stall Characteristics

One of the central aspects of the EBF–DEP system is its ability to delay stall through slipstream energization. The upcoming simulations will analyze streamline curvature, pressure distribution, and local Reynolds number variations to determine the onset and nature of stall for different configurations.

Structural and Thermal Considerations

Following aerodynamic optimization, a preliminary structural analysis will be conducted to assess the impact of high-lift loading on the wing–flap assembly. Thermal effects arising from motor operation and distributed power electronics will also be briefly examined for feasibility.

Feasibility Analysis

The design of the propulsion system needs to be realistic. For this study, we have ignored the weight of the battery pack required to sustain flight. In the future analysis, we will also look at the power required to generate the thrust according to design, and consequently the battery weight must also be included (apart from the payload). This report majorly focused on the takeoff portion of the mission. We must also cover the cruise requirements in order to achieve a feasible model.

References

[1] D. A. Spence, "The lift on a thin aerofoil with a jet-augmented flap," *The Aeronautical Quarterly*, vol. 12, no. 3, pp. 287–299, 1961.

[2] D. R. Agrawal, F. As'ad, B. Berk, T. Long, J. Lubin, C. Courtin, J. Thomas, R. J. Hansman, and M. Drela, "Wind tunnel testing of a blown flap wing," in *AIAA Aviation 2019 Forum*, (Dallas, Texas), AIAA, 2019. AIAA Paper 2019-3382.

[3] P. M. Sforza and R. R. Smeltzer, "Analysis of the aerodynamics of a deflected slipstream powered-lift system," Tech. Rep. NASA TN D-3584, NASA Langley Research Center, Hampton, Virginia, 1966.

[4] C. E. Brown and J. Michael, William H., "On slender delta wings with leading-edge separation," Technical Note TN 3430, National Advisory Committee for Aeronautics (NACA), 1955. Document ID: 19930084288, Accession Number: 93R13578.

[5] R. E. Kuhn, "Investigation of the effects of propeller slipstream on the aerodynamic characteristics of wings," NACA Research Memorandum RM L56E30, NASA, 1956.

[6] C. B. Courtin and R. J. Hansman, "An assessment of electric stol aircraft," Master's Thesis Report ICAT-2019-13, Massachusetts Institute of Technology, International Center for Air Transportation (ICAT), Cambridge, MA, USA, August 2019. Based on the Master's Thesis of Christopher B. Courtin submitted to MIT Department of Aeronautics and Astronautics.

[7] T. Long, "An experimental investigation of propeller blown-flap airfoils," master's thesis, Massachusetts Institute of Technology, Department of Aeronautics and Astronautics, Cambridge, MA, USA, August 2021.

[8] M. Dumont, "Conceptual approach to blown wing aircraft: Design and performance estimation – based on reverse engineering insights," master's thesis, Université de Liège, Faculté des Sciences Appliquées, 2024. Master en ingénieur civil en aérospatiale, à finalité spécialisée en "aerospace engineering".

[9] AirfoilTools.com, "Airfoil database and analysis tools," 2025.

[10] APC Propellers, "Apc propeller performance data," 2025.